High-Frequency Propagation and Failure of Asymmetric Half-Disk Field Access Magnetic Bubble Device Elements

LASZLO GAL AND FLOYD B. HUMPHREY, FELLOW, IEEE

Abstract—**High-frequency propagation characteristics and failure modes in 14-μm period, 1.8-μm gap, asymmetric half-disk field-access device were studied using a high-speed optical sampling technique. Propagation elements as well as normal and hand gun corners and chevron structures were included. The operating bias margin at 1 MHz, for a structure that had 1.2 MHz as highest possible frequency, was about half of the margin for frequencies of 200 kHz and below. The phase lag between the bubble leading wall and the instantaneous rotating field direction was nearly 90° as the bubble moved through the center of the element where the lag was the greatest. The peak velocity of the leading wall of 55 m/s and the trailing wall of 46 m/s is attributed to bubble interaction with the Permalloy structure creating a ~125 Oe in-plane field that greatly increases the free bubble "saturation" velocity.**

INTRODUCTION

HIGH-FREQUENCY device testing has generally dealt with the frequency limit of either a complete chip or a test loop. On the other hand, free bubble measurements have emphasized the mobility, peak, or saturation velocity with only limited success in relating the free bubble dynamic characteristics with the velocity of a bubble in a device. This lack of success is primarily because the motion of a bubble along a device structure is an extremely complicated one. The bubble exhibits erratic motion with extreme changes in velocity. Using an optical sampling technique, Kobayashi *et al.* [1] actually watched the bubble move through a device structure. Instantaneous velocities well above any expected theoretically were observed. It was suggested that the applied in-plane field and the field generated by the Permalloy structure might be the reason that such high velocities were found. A phase lag change as the operating frequency was changed from 100 kHz to 200 kHz was also observed. This observation of phase was also made by Il'yashenko *et al.* [2] using a stroboscopic technique that measures directly the in-plane drive direction as a function of instantaneous bubble position through the device cycle. More recently, Doyle *et al.* [3] investigated the high-frequency characteristics of test loops of gap-tolerant half-disk type structures. They compared the free bubble parameters to the high-frequency performance of their device by making observations as a function of temperature. They concluded that the high-frequency limit of circuits on YSmLuCaGe garnet is most consistent with the limitation caused by the saturation velocity of the material. This value is obtained using the empirical formula of de Leeuw [4]. Recently, Speriosu *et al.* [5] made a very complete analysis of the bubble moving in an asymmetric half-disk propagation element. The frequency for this study, however, was well below that where any high-frequency effects would be expected. Here we address that high-frequency question by observing the same elements at the edge of their high-frequency limit. An attempt to relate this high-frequency performance to the free bubble characteristics will be made. The device failure modes will also be investigated, qualitatively, by observing outside of the range of stable operation.

Manuscript received December 1, 1978; revised February 26, 1979. This work was supported by the National Science Foundation Division of International Programs under Grant INT 76-02666 and by the Division of Materials Research under Grant DMR-77-24024.

L. Gal was with the California Institute of Technology, Pasadena, CA 91125, on leave from the Central Research Institute for Physics, Academy of Sciences, Budapest, Hungary.

F. B. Humphrey is with the California Institute of Technology, Pasadena, CA 91125.

EXPERIMENTAL

An optical sampling microscope was used in the measurements [1], [5]. A detailed description of the optical sampling system can be found elsewhere [6]. The image of the moving domain illuminated by a single 10 ns light flash is recorded on video tape using a silicon intensified target video camera. Simultaneously, the sample is illuminated in the transmission mode by a weak incandescent lamp that allows the Permalloy elements to be seen. The same kind of half-silvered mirror was used as in [5] to avoid the interference caused by the propagating structure. The rotating field was produced by a pair of flat orthogonal coils with small inductance. A burst of two cycles of rotating field was used with the light flash synchronized so that it occurred at various times through the second cycle. The repetition frequency was never larger than 60 Hz so that the duty cycle of the rotating field would be so small that no heating effect of the coil would be obtained. Although a longer burst would have facilitated the comparison of the results here with those of others, avoiding a temperature problem was felt to be more significant. Since we actually see the bubble here, we can be assured that the effect of the start operation is mainly important in the first cycle. All of the measurements were made at room temperature (25°C).

The rotating field was provided by two small perpendicular coil pairs. The voltage drive was triangular which leads to current drive that is nearly sinusoidal because of the coil inductance. Deviation from the linear relationship between the angle of the rotating field and time was less than a few degrees at all frequencies involved. No jitter existed between the laser

0018-9464/79/0700-1113$00.75

light flash and the rotating field pulses. During the investigation of the failure modes a bias modulation coil was also used synchronized with the rotating field. The nominal composition of the garnet film in this study was $(YSm)_3(FeGa)_5O_{12}$. Its thickness, demagnetized stripe width and collapse field are 3.55 μm, 3.86 μm, and 110 Oe, respectively, giving a length parameter of $l = 0.452$ μm and magnetization of $4\pi M = 230$ G. As measured by ferromagnetic resonance, the anisotropy field is 1200 Oe, resonance damping $\alpha = 0.08$ and $\gamma = 1.78 \times 10^7$. A value of $A = 1.4 \times 10^{-7}$ ergs/cm is used in calculations [7]. The device is a fully implemented 100 kbit single loop shift register with a 14-μm period, a 1.8-μm gap, and a 1.3-μm circuit to garnet spacing. It is the same device that was investigated previously [5].

Results and Discussion

The transient shape of a bubble propagation through a cycle on an asymetric half-disk element can be seen in Fig. 1. This figure is a composite that was constructed from single 10-ns exposure time pictures taken in an optical sampling mode in synchronism with the drive field. The bubble is propagating from right to left in the figure and the drive is rotating counterclockwise. The instantaneous direction of the 42-Oe drive field is indicated by arrows on the diagram. Fig. 1(a) is for a propagation frequency of 200 kHz and Fig. 1(b) is the same element driven at 1 MHz. The bias field is 100 Oe, which is essentially the center of the 34-Oe margin at 200 kHz or 16-Oe margin at 1 MHz. It can be seen in Fig. 1(a) that there is some elliptical distortion of the bubble and some size variation. The phase of the bubble motion compared to the drive field is less than 15° lag at all times. The size variation and phase at 148 kHz have been analyzed by Speriosu *et al.* [5], and the results here at 200 kHz are consistent with their analysis.

The transient shape of the bubble moving at 1 MHz can be seen in Fig. 1(b). The upper propagation frequency limit of this element is 1.2 MHz, so that 1 MHz is high enough to allow the effects of the high frequency to be observed, yet far enough from the upper limit to have stable operation. In making this composite, bubbles were chosen that illustrated the bubble shape and position during a cycle rather than choosing bubbles at equal intervals. The instantaneous 42-Oe drive field direction is indicated by arrows. It can be seen that the bubble path shifts towards the outer edge of the half-disk requiring the bubble to go farther at higher frequencies. The size variation increases from about 1:2 at 200 kHz to 1:3 at 1 MHz. The round bubble elongates while crossing the gap, becomes a long ellipse on the "thick" leg, and then shrinks as it moves along the back of the half-disk element. It becomes round again and very small on the "thin" leg before it seems to sit on the end of the thin leg, as it did at 200 kHz, growing larger before jumping the gap. By far the greatest change that occurs as the frequency is increased is the change in phase. It can be seen that the bubble is lagging behind the drive field by nearly 90° along the back of the element where the phase lag is the largest. It is clear that the phase determines the stable operation and, if it becomes greater than 90°, the bubble loses synchronism. This condition will occur at 1.2 MHz as the bubble moves along the back of the element.

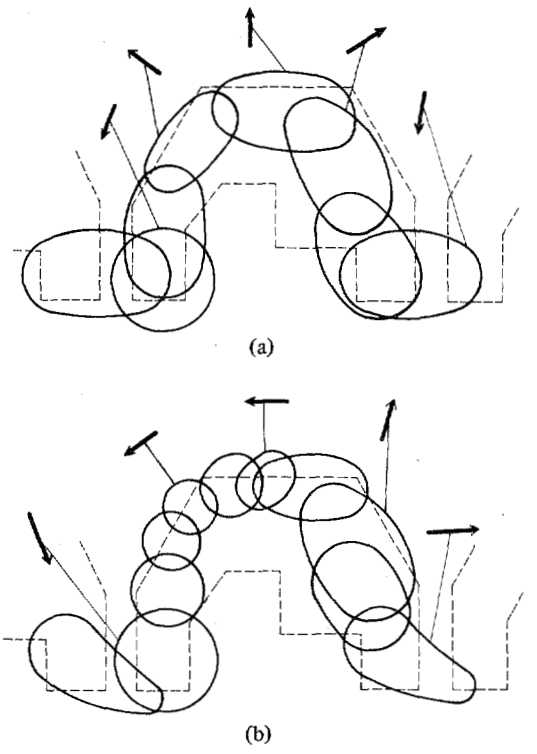

Fig. 1. Transient shape of a bubble propagating on a half-disk element at (a) 200 kHz and (b) 1 MHz as seen looking through the substrate with the half-disk element indicated by dashed lines in the background. The arrows indicate the instantaneous direction of the rotating in-plane drive field; bias is 100 Oe.

The instantaneous velocity of the bubble as it moves through one cycle as a function of the angle of the drive field is plotted in Fig. 2 for a bias of 94 Oe. This bias setting, near the lower margin, was chosen to emphasize the distortion. The position of the wall is indicated on the abcissa with letters corresponding to the position on the half-disk element, as shown, where the velocity was measured. The dashed line indicates the free bubble "saturation" velocity of the material. The angle reference for the 1 MHz, 42 Oe drive field is also indicated. The upper graph is for the leading edge of the bubble and the lower graph is for the trailing edge. The instantaneous velocity was obtained by observing the distance the bubble seemed to move during a 50-ns (18°) change in the sampling time. Even though the distortion is large, the shape is reproducible, cycle by cycle, so that the instantaneous velocity is not affected by the fact that different bubbles are used to determine the distance moved. The leading or trailing edge was determined at a given time and the shortest distance to the wall of the bubble in the previous sample was used to calculate the respective velocity. It can be seen that the velocity exhibits large variations similar to what was seen at 148 kHz [5] and in other elements [1] using the same technique. It is, however, the leading edge that exhibits this velocity variation since the trailing edge velocity at 1 MHz is much more uniform than the trailing edge velocity at 148 kHz [5] on the same element. However, with the large phase difference it is unreasonable to compare the position of

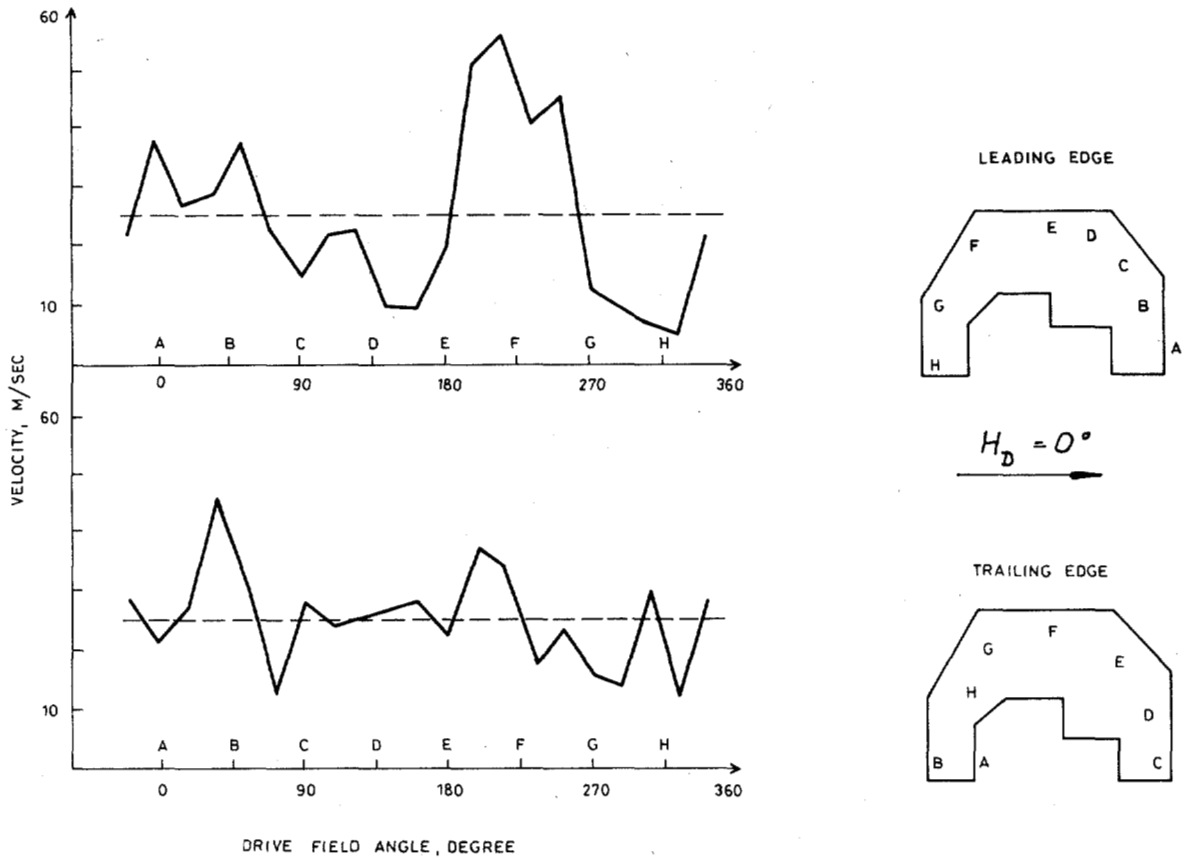

Fig. 2. The instantaneous velocity and position of the leading edge (upper graph) and trailing edge (lower graph) of a bubble as a function of the angle of the 1 MHz, 42 Oe drive field. The bias is 94 Oe.

the velocity peaks in the drive field angle even though the angle scale uses the same reference direction. When the position of the bubble on the half-disk element is used for the comparison it can be seen that there is considerable difference between the motion at 148 kHz and at 1 MHz. Three velocity peaks are reported at 148 kHz [5], one across the back of the element, another along the narrow leg, and the largest as the leading edge transverses the gap. It can be seen in Fig. 2 that at 1 MHz as the leading edge jumps the gap (H-A) the velocity is actually rather slow. As the bubble moves along the narrow leg (F-G) it is also slow and slowing. Only the large velocity peak along the back (E-F) corresponds to a low-frequency peak. The general motion of both walls is actually more uniform in the high-frequency case. The observed maximum peak in the leading edge velocity is only 2.2 times the average instead of 3.4 times the average velocity observed at the lower frequency and for the trailing edge the highest velocity is only 1.8 times the average, whereas the trailing edge followed the leading edge at low frequency. This difference in bubble motion at the two different frequencies is reasonable if it is assumed that the velocity peaks are caused by two different mechanisms. At low frequencies it is reasonable to assume that they are caused by discontinuous changes in the effective drive field from the permalloy structure. The largest observed velocity peak occurred when the potential well was supposedly moving the slowest in the cycle [8]. At high frequency, however, the leading edge moves fast when it has a long way to go to keep up with the fast moving potential well.

A very attractive model for the high-frequency behavior of propagating structures is one that recognizes velocity fluctuations during a propagation cycle and assumes failure when one of these fluctuations reaches some limiting velocity that is given by the free bubble characteristics. The difficult question that such a model poses is what velocity to use. Previously, velocity peaks well above the Slonczewski critical velocity were reported for T bar, TX bar, X bar, and chevron structures [1]. As seen in Fig. 2 for the asymmetric half-disk structure, the leading edge goes 55 m/s along the back of the thin lag and the trailing edge moves 46 m/s pulling away from the gap. These velocity peaks are again much higher than the Slonczewski critical velocity v_p = 16 m/s for this material. Doyle *et al.* [3] concluded that the limiting velocity was the saturation velocity of the material and suggested using de Leeuw's empirical formula to obtain the value of it. For this material $v_s = 0.5\ \gamma\sqrt{A/Q} = 14$ m/s, which is even poorer agreement than v_p. It is interesting to note that this same poor agreement is obtained for other structures [1] where peaks of 25 m/s were seen with material where the de Leeuw formula gives v_s = 6 m/s. It is clear that none of the proposed peak of saturation velocities are appropriate for high-frequency behavior.

The free bubble radial expansion [9] velocity is shown in Fig. 3 where the velocity is plotted as a function of applied pulsed bias field. Curve (a) is without an in-plane field and

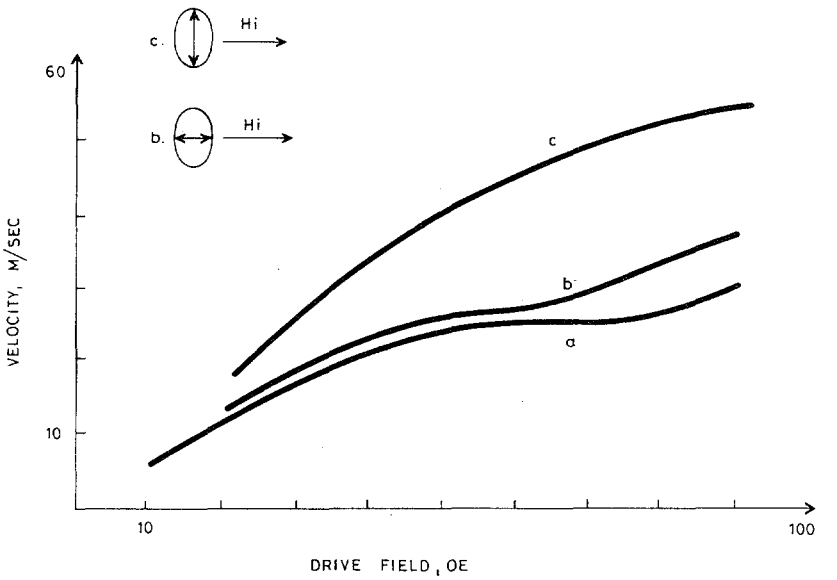

Fig. 3. Free bubble radial expansion velocity as a function of the drive field. a—Without in-plane field. b—With 100 Oe in-plane field parallel to wall motion. c—With 100 Oe in-plane field perpendicular to the wall motion.

curves (b) and (c) are with a 100-Oe constant in-plane field. The velocity in the two directions with respect to the in-plane field is indicated in the insert. It can be seen by curve (a) that the velocity without in-plane field generally changes with drive; however, there is a small plateau between 50 and 80 Oe which can be taken as a "saturation" velocity and is the value used in Fig. 2 (dashed line). It is clearly unrealistic to attempt to explain the 55 m/s observed wall velocity with curve (a) since completely unreasonably high drive fields would be required of the Permalloy to account for the observed high velocity. Considering the fact that the bubble is small when it is moving fast, it is perhaps possible to imagine gradients of 43 Oe/μm corresponding to a radial expansion pulse drive field of 50 Oe. Such an estimate comes from the desire to at least get up on to the plateau of curve (a). Certainly such high gradients cannot be extracted from quasi-static device modeling calculations [8].

An in-plane field on the bubble, as was previously suggested [1], must be the important factor in explaining the high velocity observed; however, such an explanation is not simple. The drive field can immediately be dismissed as ineffective in supplying this field. An in-plane field of 50 Oe made no noticeable effect on the wall velocity shown in Fig. 3 with curve (a). With 100-Oe in-plane field, however, a significant increase in the wall velocity was found, however, with a large velocity anisotropy. The velocity of the walls moving perpendicular to the in-plane field increased (curve (c)), but the velocity of the wall moving parallel (curve (b)) did not. This effect of the in-plane field on the wall velocity is consistent with the results of Vural and Humphrey [10] who have recently looked in detail at the radial wall velocity over a wide range of effective drive fields and in-plane fields. They found that the velocity depends on the in-plane field nearly exponentially and that a velocity anisotropy exists for in-plane fields less than $4\pi M$. It can be seen from Fig. 3 that, by assuming a gradient greater than 30 Oe/μm and an in-plane field somewhat over the 100-Oe curve shown (~125 Oe), the observed device velocity should be expected; however, the in-plane field cannot be paralled to the wall motion (curve (b)). Considering the nearly 90° phase lag, this assumed in-plane field must have a substantial component normal to the instantaneous drive field direction.

If there is any correlation between the free bubble expansion velocity and the bubble translation velocity in a device, it is necessary to postulate that the required fields are supplied by the Permalloy structure. Such a suggestion subjects the Permalloy to quite different conditions than is usually done in device modeling [8]. The bubble moves out from its equilibrium position under the Permalloy element as the frequency is increased, presumably because of the gyroscopic forces on it. These forces are not included in usual device modeling calculations, however, the assumption that the forces are significant is reasonable since we have confirmed that $S = 1$ bubbles are the stable species in this material and the influence of the gyroscopic force on device operation has been seen in other elements [11]. The direction of field rotation and bubble magnetization is consistent with this assumption. At the edge of this wide Permalloy element, the strong stray fields from the bubble must magnetize the Permalloy creating an effective pole distribution that supplies both the driving gradient as well as the in-plane component required by Fig. 3(c). Dynamic equilibrium at this location must involve a balance between the two factors that determine the wall velocity, i.e., the gradient and the in-plane field. Displacement across the Permalloy edge gives a restoring force to balance the gyroscopic force, however, increased overlap of the edge decreases the available drive field gradient while increasing the in-plane component. It is this balance among these factors that ultimately determines the maximum operating frequency of the device.

The importance of the in-plane field can be seen by the chance observation of the stripe tail velocity seen in Fig. 4. These pictures were taken during the failure mode study that will be discussed later; at this time it is of interest to observe

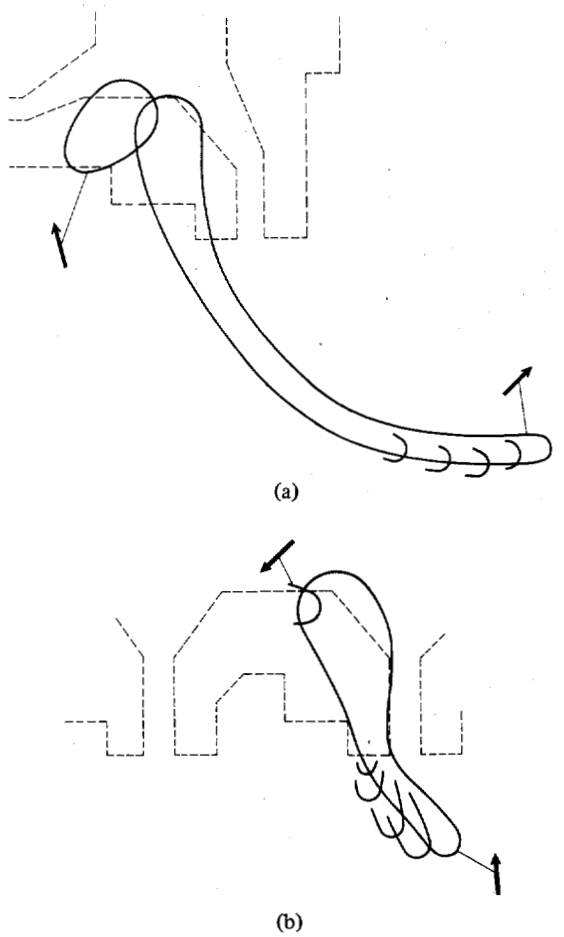

Fig. 4. (a) Stripe head motion far from a corner structure at 200 kHz. (b) Stripe head motion in the vicinity of a long row of half-disk elements at 1 MHz. The arrows indicate the direction of the drive field.

the motion of the tail of an elongated bubble under two different circumstances. In each case the original elongated bubble is shown as well as the positions of the tail as it contracts. Fig. 4(a) shows a long stripe at the end of the shift register, well away from the influence of the Permalloy. The stripe is contracting at 24 m/s in good agreement with the free bubble radial expansion "saturation" velocity. The shorter stripe shown in Fig. 4(b) is on a half-disk element in the vicinity of a large amount of Permalloy. The stripe contraction velocity is 42 m/s just as the drive field (rotating ccw) develops a component along the row of elements. It is reasonable to assume that the Permalloy element produces an in-plane field that is the significant factor in the observed wall motion.

The operation margin for the various elements investigated at various frequencies is listed in Table I. This table is included in an attempt to give the reader an indication of the relative differences between these elements at various frequencies. The information is self-consistent, however, care should be used in attempting to compare to the results of others because of the very different operational definition of failure. From Table I it can be seen that there is no margin change for frequencies below 200 kHz; however, by 1 MHz the margin has reduced by a factor of two. Failure at the upper margin was by bubble collapse at the position of the smallest bubble in

TABLE I
BIAS MARGIN AT A DRIVE FIELD OF 42 OE AT DIFFERENT FREQUENCIES

	1 MHz	500 kHz	200 kHz	62.5 kHz
Propagation	92–108	86–113	84–118	84–118
Normal corner	95–108	95–115	93–120	93–120
"Hand-gun" corner	94–108	88–113	82–118	82–118

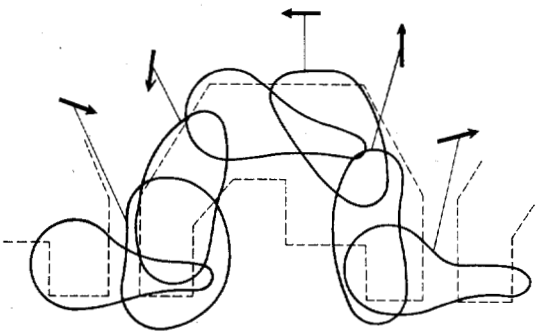

Fig. 5. Transient shape of a bubble propagation on a half-disk element at 1 MHz and 1 Oe above the lower margin as viewed through the substrate. Arrows indicate the direction of the drive field.

Fig. 1(b). The corner structures contain the half-disk and were similar. The failure was very simple; as the bias field increased, the size of the small bubble decreased until it collapsed 2 Oe above the free bubble collapse field. At the lower margin, the failure was more interesting. Fig. 5 is a composite in the style of Fig. 1 but with the bias field 1 Oe above the lower margin. The leading edge of the bubble is only slightly effected by the lower bias field and the phase for it is essentially that of the margin center (Fig. 1(b)). The trailing edge lags well behind during the entire cycle. The elongation is particularly extreme along the back and across the gap. It is the stretching across the gap that will ultimately lead to failure.

The particular mode of failure at the lower margin depends upon the pattern in the propagating structure. As the tail grows, the phase lag becomes extreme. Finally, the poles at the end of the thin leg repel the tail as can be seen in Fig. 6(a). This transient photograph was taken with the drive field angle as shown, just as repulsive poles should develop on the end of the thin leg. When there is a vacant position along the track, the long tail is attracted to it either from the adjacent position of the same row or from the next row. This failure can be seen in Fig. 6(b). If every position of the shift register is filled, the tail swings out and finally cuts off, as can be seen in Fig. 6(c), forming excess bubbles. Consistent with the observation of Doyle *et al.* [3], these lower margin failures always produce extra bubbles.

The corner structure failure mechanism is similar to propagation track failure. The corners used in our experiments and the early phase of the failure is shown in Fig. 7. The tail of the bubble develops when the front of the bubble moves on the thick leg of the half-disk. When the corner is formed with "hand-gun" elements, as in Fig. 7(a), the geometry is not

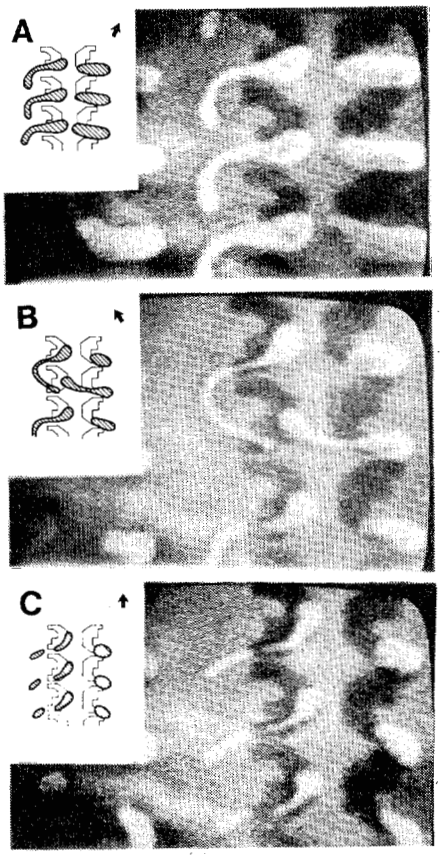

Fig. 6. Lower margin propagation failure in a half-disk element at 1 MHz. (a) In the early phase of the failure a long tail of the bubble is developed. (b) Extra bubbles go into the next cell if there is a vacancy. (c) Extra bubbles are formed outside the structure if every cell is filled.

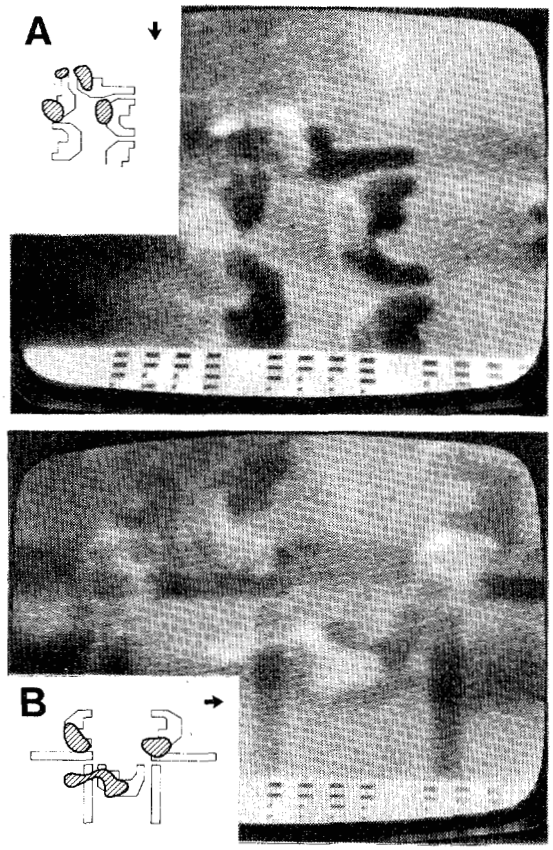

Fig. 7. Propagation failure of bubbles. (a) In "hand-gun" corner. (b) Normal corner structures at 1 MHz and at the lower bias margin. The instantaneous drive direction is indicated.

favorable for the tail of the bubble to stretch into the adjacent cell even if it is vacant. Therefore, the extra bubbles formed by the long tail were always found outside of the shift register. The normal corner structure consisting of one half-disk and long I bars behaves quite differently as can be seen in Fig. 7(b). Since the long I bars can develop strong poles at their ends even when there is only a small component of the drive field along their long axis, the tail is always affected by these bars. As the cycle continues a little more than 180° from the situation in Fig. 7(b), the tail of the lower bubble slides down the center I bar to the end, as the head of the bubble reaches the end of the thin leg. Note that the head of the bubble exhibits the same 90° phase lag as seen on the propagation structures. Even though the normal corner seems insensitive to the higher frequency as far as the lower margin is concerned (see Table I), it is clearly having a more difficult time operating at the higher frequency than the "hand-gun" corner because the long tail of the bubble domain must keep up with the fast movement. Probably the lower margin failure of the test loops with normal corners reported by Doyle *et al.* [3] was failure at the corner.

Chevron elements were examined although the same systematic study as was done on the half-disk was not made. The propagation of stripes on the chevron structures is generally so peculiar that quantitative analysis at higher frequencies was not attempted. The propagation of a stripe in a 5-element chevron structure can be seen in Fig. 8 at the center of the bias margin. As can be seen, the head follows the fast moving

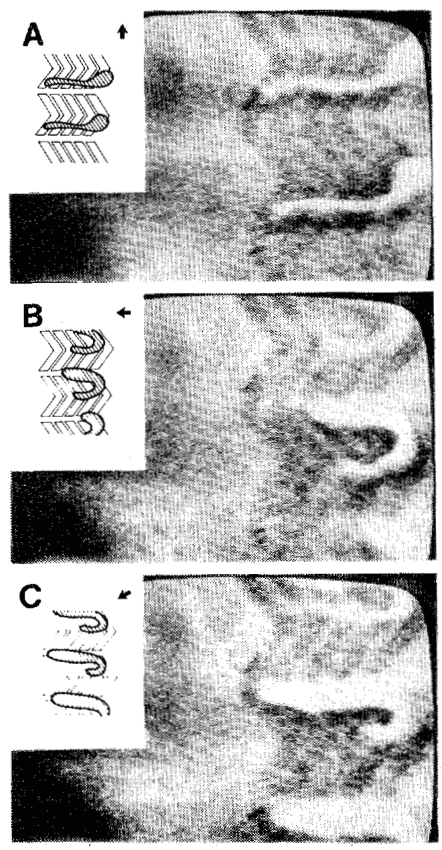

Fig. 8. Stripe propagation on a 5-element chevron structure at the center of the margin at 1 MHz. The instantaneous drive direction is indicated.

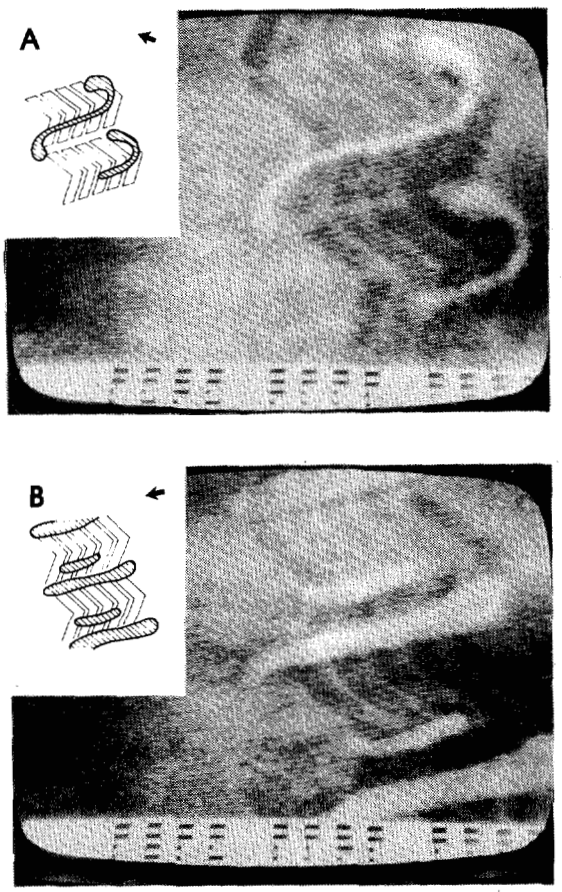

Fig. 9. Stripe propagation failure at the lower margin on a 5-element chevron structure at 1 MHz. The instantaneous drive direction is indicated.

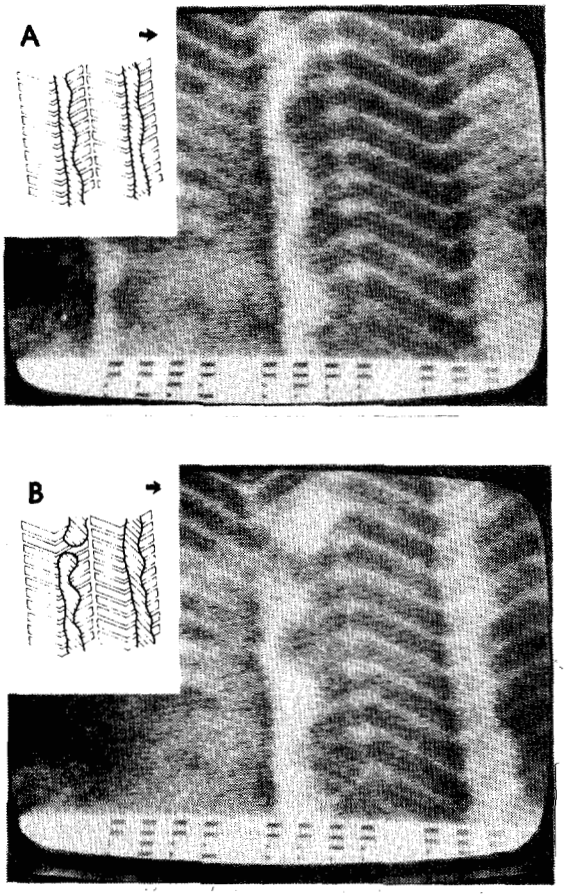

Fig. 10. Stripe propagation failure in the center of a 120 element chevron expander showing (a) width instabilities and (b) stripe breakup. The instantaneous 1 MHz drive direction is indicated.

potential well with a phase lag of about 90° in the three pictures shown in Fig. 8(a), (b), and (c), where the direction of drive field is indicated. A large "tail" is lagging behind in Fig. 8(a). The phase lag of this tail is so large (>90°) that it is out of synchronism and cannot follow the head but shrinks and curls as can be seen in Fig. 8(b). The head then moves out along the structure to form a stripe again as in Fig. 8(c). The tail then becomes the head for the next cycle. Even though the distances are longer, the large phase lag forces the bubble to tumble through the structure.

Failure of propagation on the chevron structure at the lower margin is illustrated in Fig. 9. The long tail develops as shown in Fig. 9(a). It cannot shrink fast enough to follow the head so it is cut off. As can be seen in Fig. 9(b), it rides along between the heads that are now stripes. Note that the upper short bubble in the center of the upper chevron is the tail for the upper head just out of sight. The tail for the center head is the lower short stripe. If the track is full, the tail then unites the next stripe; however, if the position is vacant, then it fills that position. Extra bubbles are created but always within the structure.

Failure in long chevron structures can be seen in Fig. 10. This picture is near the center of a 120-chevron step expander fed from the center. The third and fourth columns are shown. It can be seen that the motion is erratic, even though it is biased in the margin center, since both Fig. 10(a) and (b) are taken at the same drive field angle. In Fig. 10(a), instabilities in width can be seen that are similar to those seen at low frequency with low drive field. These instabilities are found at all times through the cycle except when the stripe is in the gap. Certainly, such distortions could effect the detector operation. It can also be seen in Fig. 10(b) that the stripe does not remain continuous but breaks up. Once broken, the stripe continues to propagate as a broken stripe.

Conclusion

It is concluded that the high-velocity peaks existing during the propagation of bubbles in devices at high frequency require enhanced gradient drive fields with a large in-plane component normal to the instantaneous drive direction. Both the in-plane field and the enhanced gradient must come from bubble-permalloy interaction. Although the saturation velocity modified by the in-plane field was used, no theoretical or empirical formulation by others was found to give reasonable agreement with the device or free bubble measurements. Failure occurs at the upper margin by simple bubble collapse and at the lower margin because the phase between the tail and the drive field is much greater than 90°.

Acknowledgment

We would like to thank the Bubble Group at Rockwell International, particularly T. Kobayashi and P. J. Besser, for providing the sample and their discussion and encouragement during this study.

References

[1] T. Kobayashi, P. K. George, and F. B. Humphrey, *IEEE Trans. Magn.*, vol. MAG-12, pp. 202, 1976.
[2] E. I. Il'yashenko, S. N. Matveyev, and N. J. Karmatsky, *J. Appl. Phys.*, vol. 49, p. 1933, 1978.
[3] W. D. Doyle, R. M. Josephs, and A. B. Smith, *IEEE Trans. Magn.*, vol. MAG-14, p. 303, 1978.
[4] F. H. de Leeuw, *IEEE Trans. Magn.*, vol. MAG-14, p. 596, 1978.
[5] V. Speriosu, Y. Rosenthal, F. B. Humphrey, and T. Kobayashi, *IEEE Trans. Magn.*, vol. MAG-15, Jan. 1979.
[6] F. B. Humphrey, *IEEE Trans. Magn.*, vol. MAG-11, p. 1679, 1975.
[7] J. T. Carlo, D. C. Bullock, and F. G. West, *IEEE Trans. Magn.*, vol. MAG-10, p. 626, 1974.
[8] W. Ishak and E. Della Torre, *IEEE Trans. Magn.*, vol. MAG-14, p. 1035, 1978.
[9] G. J. Zimmer, L. Gal, K. Vural, and F. B. Humphrey, *J. Appl. Phys.*, vol. 46, p. 4976, 1975.
[10] K. Vural and F. B. Humphrey, *J. Appl. Phys.*, to be published.
[11] H. Matsutera and Y. Hidaka, presented at the Conf. on Mag. Mat. Cleveland, OH, paper 6B6, Nov. 1978.

Optoelectrical Study of Bubble Propagation in Field Access Devices

E. I. IL'YASHENKO, S. N. MATVEYEV, N. I. KARMATSKIY, YE. P. PARINOV, AND G. K. CHIRKIN

Abstract—**Bubble propagation on several field access structures is studied with an optoelectrical method. Measurements were performed with a 40-Oe, 10-kHz rotating field on closed-loop shift registers that were fabricated on Bi-substituted garnet films having either 7 μm or 2.7 μm bubbles. The effect of increasing the interelement gap for several nonsymmetrical structures is discussed.**

Introduction

SEVERAL METHODS for studying the motion of bubbles on propagate structures have been reported previously [1]-[4]. In addition, an optoelectrical method has been reported [5] that permits a) the direct determination of $\theta = f(X)$ where θ is the phase difference between the angular position of the center of the bubble and the rotating field H_r and X is the position coordinate of the center of the bubble; b) direct measurement of bubble size fluctuations along the path; and c) the photographing of time-averaged trajectories.

In this paper we report on the use of the optoelectrical method for studying and comparing the characteristics of several popular bubble propagate structures.

The Experimental System

The experimental circuits were made of closed-loop shift registers of a 20- or 30-bit capacity having different geometrics and periods. The circuits were fabricated in the following sequence: 1) a 1200-Å film of aluminum was sputtered on a Bi-substituted epitaxial garnet film; 2) a 5000-Å SiO_2 film was deposited on the aluminum film; and 3) finally, a 4500-Å Permalloy film was sputtered on the SiO_2 and patterned. The unpatterned aluminum film serves as a mirror to enhance the observation of the bubble motion in reflected light [6].

Our experimental system consists of a conventional polarization microscope with built-in epi-illumination, a bias field coil and rotating field coils to produce H_r. The domains are observed visually or with a photomultiplier (PEM). The PEM output is connected to the Z, or beam intensity, input of a conventional oscilloscope which has its X and Y inputs driven by the X and Y rotating field coils. From such a display $\theta = f(X)$ can be obtained as has been described in detail in [5].

In all experiments the rotating field frequency was 10 kHz. The bubble tracks were photographed with an exposure time of 10 s with bubbles in every position. The θ-characteristics were also determined with bubbles in every position. The θ-characteristics of the structures with bubbles in every position and in every other position were found to be approximately identical.

Experimental Results and Discussion

In at least one structure the potential well continuously moves with the bubble while a uniformly rotating drive field H_r is applied. Fig. 1 portrays this structure of [7] and a track of bubble propagation along it. Analysis of the path of Fig. 1 and the output of the PEM which "views" this track through a slot reveals that there is no position of such a structure where the bubble stops although its velocity increases with the curvature radius of the drive structure and the bubble size varies noticeably.

Bubble tracks along $T-1$, $I-1$, $T-X$, $Y-1$, and other similar structures contain halted bubbles of different degrees of contrast. This confirms the existence of nonuniform jerky motion of the potential well and thus of the bubble and the

Manuscript received July 17, 1978.
The authors are with the Institute of Control Sciences, Moscow, USSR.

0018-9464/79/0700-1120$00.75